JOURNAL OF AGRICULTURAL AND FOOD CHEMISTRY

pubs.acs.org/JAFC

Article

First Characterization of the Formation of Anthocyanin−Ge and Anthocyanin−B Complexes through UV−Vis Spectroscopy and Density Functional Theory Quantum Chemical Calculations

Laura Estévez,* Marta Queizán, Ricardo A. Mosquera, Lucia Guidi, Ermes Lo Piccolo, and Marco Landi*

Cite This: *J. Agric. Food Chem.* 2021, 69, 1272−1282

Read Online

ACCESS | Metrics & More | Article Recommendations | Supporting Information

ABSTRACT: The occurrence of anthocyanin (ACN) and metal (Me) complexes has been widely supported by many research works while the possibility that ACNs bind to metalloids (Mds) is yet to be proven. Here, metalloids (H_3BO_3 for B; GeO_2 for Ge) were added to cyanidin-based solutions at pH 5, 6, and 7 and ACN−Md stoichiometric ratios of 1:1, 1:10, 1:100, and 1:500, and UV−vis transmittance spectroscopy as well as density functional theory (DFT) calculations were performed to test this hypothesis. Ge and B addition caused bathochromic and hyperchromic shifts on ACN UV−vis spectra, particularly pronounced at pH 5 and a 1:500 (ACN:Md) ratio. ACN−Me complexation reactions have been evaluated where Ge showed a higher capability to bind to ACNs than B. Among the complexes envisioned, those labeled as **b1**, **b2**, and **b3** feature UV−vis spectra compatible with experiments. The combination of experimental and computational data offers for the first time evidence of the formation of ACN−Md complexes.

KEYWORDS: *anthocyanin−metalloid complex, bathochromic shift, hyperchromic effect, molecular absorption simulations, molecular modeling*

INTRODUCTION

Anthocyanins (ACN) are a conspicuous class of water-soluble pigments (ranging from pale pink, to red−purple, and blue) which are responsible for the marvelous color versatility of the plant kingdom.[1] ACN belongs to the family of flavonoids, likely the most studied pathway of secondary metabolism *in planta*[2] and are synthesized in a wide range of plant cell and tissues of different plant organs including leaves, flowers, fruits, roots, tubers, and stems.[3−5]

Anthocyanins are di or trihydroxy B-ring-substituted flavonoids containing a flavylium cation which, owing to its conjugated double bonds, absorbs visible light with a peak in the 500−550 nm waveband.[6] The wide range of anthocyanin-derived colors depends on the degree of hydroxylation and the number and/or type of substituted groups. To date, 17 anthocyanidins have been isolated, but most of these are found only in reproductive structures and only six aglycones (cyanidin, delphinidin, malvidin, pelargonidin, peonidin, and petunidin) have been identified in vegetative organs.[7] In addition, though only simpler anthocyanins have been considered to be present in leaves (with respect to those in flowers), in recent years some findings have opened the possibility that anthocyanins are present also in leaf tissues as most complex structures. For example, acylated anthocyanins with hydroxycinnamic acids were found in sweet basil leaves, which, beside strong absorbance in visible wavebands, also increased the UV absorbance.[8]

The different color of the anthocyanins depends on the pH which is responsible for the protonation/deprotonation of the flavylium ion, which predominates at pH < 2 and shows red color, whereas at pH > 2 a series of reversible (to some extent) chemical transformations occurs. For example, at pH values from 2 to 6 the hydration of the flavylium cation leads to the prevalent formation of the colorless hemiketal form, which transforms tautomerically into yellow *cis*-chalcone and isomerizes to *trans*-chalcone (Scheme 1). Proton transfer turns the red flavylium ion into a neutral quinoidal base, prevalently characterized by purple tonalities. At pH 6−8, blue forms of an anionic quinoidal base would be predominant,[6] though they would quickly experience degradation under physiological conditions.[9]

Like other dihydroxy B-ring substituted flavonoids, ACNs have the ability to bind metal ions, a property that has been exploited for a variety of purposes. For example, the metal binding ability may be used to stabilize ACNs from plant food sources, or to modify their colors for using them as food colorants.[10−12] The complexation of metals with cyanidin derivatives can also be used as a simple, sensitive, cheap, and rapid method for determination of the concentration of several metals in biological and environmental samples using UV−vis spectroscopy.[13,14]

Far less information is available on the ecological significance of ACN−metal (ACN−Me^{n+}) complexes in plant-environment interactions. For example, metallo-antho-

Received: October 28, 2020
Revised: December 21, 2020
Accepted: January 14, 2021
Published: January 22, 2021

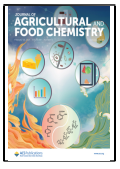

Scheme 1. pH Equilibria for the Cyanidin-3-OMe Model System[a]

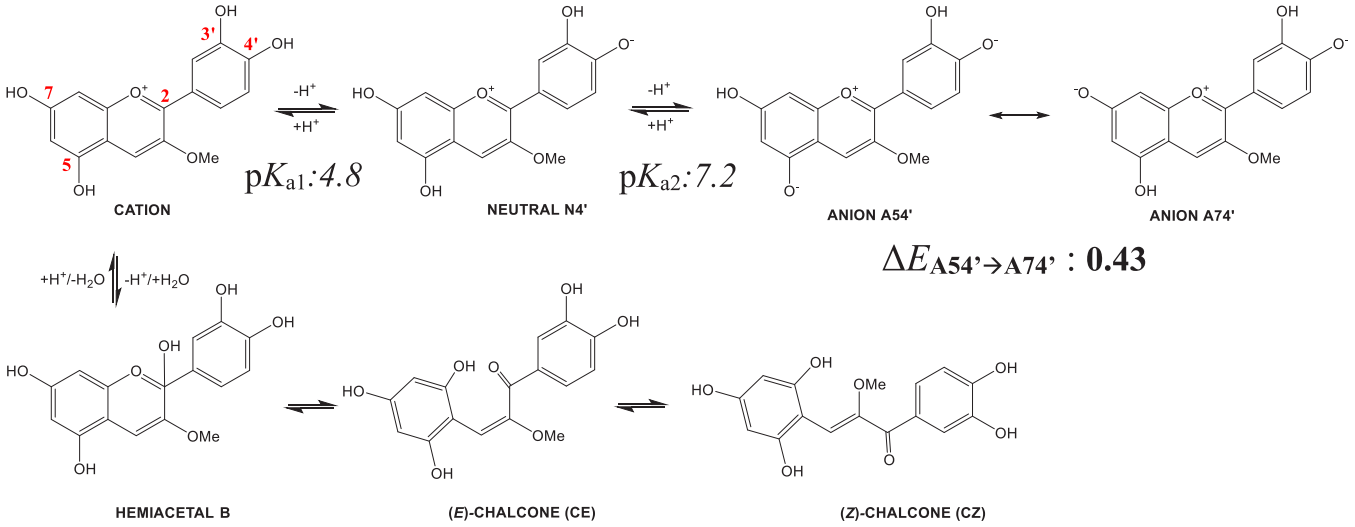

[a]Estimated (see text) pK_a values ($pK_{a1(cation \rightarrow N4')}$ 4.8 and $pK_{a2(N4' \rightarrow A54')}$ 7.2) and energy difference between tautomers of the anion form, $\Delta E_{A54' \rightarrow A74'}$ (in bold, kcal·mol^{-1}), are shown.

cyanins, supramolecular pigment complexes, consisting of stoichiometric amounts of anthocyanins, flavones, and metal ions,[15,16] are involved in the copigmentation phenomenon that leads to blue-pigmented petals, which may facilitate specific plant−pollinator interactions. However, ACN−Me^{n+} complexes have been found not only in the form of supramolecules, but also as more simple coordination compounds and ACN−Me^{n+} formation and compartmentation into the vacuole have also been proposed to be part of an orchestrated detoxification mechanism in plants which experience metal/metalloid excess.[2,17,18]

The metal-chelating ability of anthocyanins depends on the 3′,4′-O-dihydroxyl group in the B ring of the flavonoid skeleton, as also occurs for other flavonoids, such as quercetin derivatives. Binding to Me^{n+} shifts the equilibrium between different structures toward the creation of blue quinoidal form and tends to stabilize the resulting structure. Changes to the conjugation of the chromophore system of ACNs is, in turn, accompanied by chromatic changes that can be detected by UV−vis spectroscopy, which can be considered to be one of the most informative analytical tools to detect ACN−Me^{n+} complexes.[19] In addition, theoretical calculations have become ubiquitous and have given support for previous hypotheses.[20] Theoretical chemistry offers the possibility of gaining further knowledge at a molecular level of the ACN−Me^{n+} complexation process. Also, molecular absorption simulations,[21] on ACN−Me^{n+} model complexes, would help in rationalizing experimental measures with the aim of getting a deeper understanding of this interesting research topic.

Occurrence of ACN−Me^{n+} complexes have been reported for different metals including W,[22] Al,[23−26] Cd,[27,28] Cu,[29] Ga,[23,29] Fe,[30,31] Mo,[32] Mg,[26] and Zn.[28] Conversely, to the best of our knowledge, no studies have been addressed to study the possibility of ACN to form complexes with metalloids.

The aim of the present manuscript is to investigate the possibility that cyanidin-based ACN isolated from *Ocimum basilicum* cv. "Red Rubin"[8] can bind to two metalloids (Mds), namely Ge and B, with the attempt to describe for the first time the possible occurrence of such ACN−Md complexes. If confirmed, this possibility represents a first preliminary result to be confirmed *in vivo* by future experiments (requiring more complexes analyses) which could be supportive for the higher tolerance of red- than green-leafed cvs of sweet basil to B toxicity.[17,18]

In addition, though not essential for plants, in the upper continental crust of the Earth, Ge is the 54th most abundant element,[33] and the concentration of this metalloid ranges from 1.3 to 1.6 $\mu g \cdot g^{-1}$ in the soil, which can be toxic for some plant species.[34] Ge can be also recovered as byproduct from silver, copper, and zinc production or from combustion residues (fly ashes) from certain coals, which can contain considerable concentrations of Ge.[35] Given that Ge and B share similar transporters, e.g. the aquaporin HvNIP2;1,[36] and, likely as a consequence, B and Ge have similar effects in plant metabolism,[37] results of the present experiment might also be helpful to future researches dealing with ACN−Ge complexes in plants. Moreover, the results of the present experiment could be useful to exploit anthocyanin−metalloid binding capacity for environmental monitoring, for example as a cheap and reliable methodology to test metalloid accumulation in plant tissues or to generate knowledge in food science, for example to increase the stability of anthocyanins as natural dyes.

MATERIAL AND METHODS

Plant Material. Seeds of *O. basilicum* cv. "Red Rubin" were purchased from Franchi Sementi (Bergamo, Italy), and experiments were conducted under greenhouse conditions at the facilities of the Department of Agriculture, Food and Environment, University of Pisa, Pisa, Italy (43° 42′ N 10° 25′ E) during the period of June−July 2018.

The seeds were soaked in deionized water for 2 days to synchronize germination and then sown in 1.5 L pots filled with a sandy soil−peat mixture (60:40, v-v). Plants were irrigated with deionized water during the first week after sowing and afterward with a nutrient solution containing the following nutrient concentrations, developed to optimize sweet basil growth: NO_3^- 14 mM, NH_4^+ 0.5 mM, P 1.2 mM, K^+ 10 mM, Ca^{2+} 4 mM, Mg^{2+} 750 μM, Na^+ 10 mM, SO_4^{2-} 1.97 mM, Fe^{2+} 56 μM, BO_3^{3-} 23.1 μM, Cu^{2+} 1 μM, Zn^{2+} 5 μM, Mn^{2+} 10 μM, Mo^{3+} 1 μM. Electrical conductance (EC) was 3.04 dS m^{-1}; pH values were adjusted to 5.2−5.5 with diluted sulfuric acid.

https://dx.doi.org/10.1021/acs.jafc.0c06827
J. Agric. Food Chem. 2021, 69, 1272−1282

Climatic parameters were continuously monitored by a weather station placed inside the glasshouse. The minimum and ventilation air temperatures were 18 and 28 °C respectively; the maximum temperature reached up to 32−34 °C in sunny hours. Daily global radiation and mean air temperature averaged respectively 13.1 MJ m^{-2} and 28.2 °C. Leaf samples for anthocyanin extraction were harvested 21 days after sowing, frozen in liquid nitrogen, and stored at −80 °C until extraction.

Anthocyanin Purification and Quantification. Anthocyanins were purified as described by Sigurdson et al.[31] and quantitated by the pH differential method as described by Lo Piccolo et al.[38] with few modifications. Briefly, fresh leaf material (75 mg) was extracted in acidified methanol (1.0% HCl, v-v) and maintained overnight at room temperature. Their absorbance was recorded at 530 and 700 nm using an Ultrospec 2100 Pro UV−vis spectrophotometer (GE Healthcare Ltd., Chicago, IL). The final absorbance (A_f) of diluted samples was calculated as follows:

$$A_f = (A_{530} - A_{700})\text{pH 1.0} - (A_{530} - A_{700})\text{pH 4.5}$$

Total ACN content was expressed as cyanidin-3-*O*-glucoside (molar extinction coefficient of 34 300 M cm^{-1} and molecular weight 484.3 g mol^{-1}), and measurements of total anthocyanin content were conducted in triplicate.

Sample Preparation. ACN isolated from Red Rubin leaves were diluted to 50 μM concentrations in 500 mM buffers of either sodium acetate (pH 5−6) or sodium phosphate (pH 7), depending on the pH to test.

Metalloid salt (H_3BO_3 for B; GeO_2 for Ge) were diluted in distilled water to achieve the concentrations of 50 and 500 mM. These salt solutions were then added to the anthocyanin solutions in order to maintain the following stoichiometric ratios: 1:1, 1:10; 1:100; 1:500 [ACN:Md].

High molarity buffers were used to minimize the decrease in pH associated with addition of high metal excesses, and pH was monitored throughout the course of analysis. Control samples (without salt addition) were maintained at the same pH of each sample by using concentrated solutions of HCl or NaOH. All samples were kept under agitation for 20 min using an orbital shaker to favor the ACN−Md binding. Then, the samples were maintained under static conditions for further 20 min at room temperature in the dark prior to spectrophotometric analysis. Five replicates were evaluated for each sample.

Spectrophotometric Analyses. A 1 mL portion of each ACN−Md solution was used to determine their UV−vis spectra (380−700 nm) by transmittance spectrophotometry using an Ultrospec 2100 Pro UV−vis spectrophotometer (GE Healthcare Ltd., Chicago, IL). The spectra were used to point out bathochromic and hypochromic shifts of each ACN−Md solution (with respect to the control solutions). Spectra were captured with a 1 nm·s^{-1} scanning batch file, and the smoothing function was used to refine spectra graphs. The analyses were carried out at room temperature.

Computational Method and Model Chemical Systems. In order to reduce the computational cost, cyanidin-3-O-glucose is modeled replacing the glucose group attached to O3 by a methyl one as its effect in Cy−metal binding or in color change due to complexation can be assumed to be negligible.[20,25,26]

All cyanidin-3-*O*-methyl forms and their metalloid complexes with Ge/B were optimized with the B3LYP density functional as implemented in Gaussian 09.[39] The 6-31++g(d,p) basis set was employed for all atoms including the metalloid atom. Solvent effects (water) were included by means of the PCM solvation model.[40]

UV−vis spectrum simulations were carried out by means of time-dependent (TD)[41] B3LYP/6-31++g(d,p)/PCM(water) calculations on previously optimized Cy−Ge/B geometries in order to rationalize experimental data.

Ground state electron densities, $\rho(\mathbf{r})$, of selected Cy−Md complexes, were analyzed within the context of Bader's quantum theory of atoms in molecules (QTAIM),[42,43] with the AIMAll program,[44] for bonding characterization through selected descriptors as the electron density, the Laplacian of the electron density, and the total energy density, evaluated at relevant bond critical points (BCPs)—ρ_b, $\nabla^2\rho_b$, H_b, respectively—as well as integrated atomic properties as the electron charge $q(\Omega)$ and delocalization index δ(A, B) which gives the number of electrons that are delocalized between the basins of A and B.

Statistical Analyses. Results of UV−vis analyses are the mean of five replicates for each sample (n = 5). The homoscedasticity of the data was evaluated by a Bartlett's test and when necessary data were arcsine transformed prior to analyses. Values of hyperchromic and bathochromic shifts were compared by one-way analysis of variance (ANOVA) (2-tailed, p = 0.05) followed by a Fisher's least significant difference posthoc test (p = 0.05).

RESULTS

Experimental Results. Upon addition of $Ge(OH)_4$ to the cyanidin-based solutions at pH 5 in equimolar concentrations a bathochromic shift of the maximum absorbance wavelength, λ_{max}, from 535 to 571 nm ($\Delta\lambda_{max}$: 33 nm) is noted, as well as an increment in absorbance (hyperchromic effect) of 0.16, measured at 571 nm, when compared to control/cyanidin-containing control solution. Increasing the molar Cy:Ge ratio (from 1:1 up to 1:500) produces further absorbance increments [Δ_{OD} at 571 nm: 0.53 at 1:10, 0.59 at 1:100, and up to 0.66 at 1:500 ratios], but no significant shift of λ_{max} occurs ($\Delta\lambda_{max}$ 0.3 nm: Figure 1 and Table S1).

The increase of pH from 5 to 7 caused a shift of λ_{max} to longer wavelengths—571, 582, and 590 nm—representing bathochromic shifts, e.g., at a 1:10 ratio, of 36, 43, and 55 nm with regard to the corresponding control solution (Table S1). This can also be observed in Figure 2 (left) where the spectra of the 1:500 solutions at the three pH values tested are compared. It is also noted that the red shift is accompanied by hypochromic effects making solutions bluer but of less intensity (Figure 3) which makes the study at pH 5 more suitable.[11,30]

Addition of boric acid to the cyanidin-based anthocyanin solutions (Figure 2, right) results in a shorter red-shifting: at 1:500 ratios maximum OD takes place at 566 nm (B, on average). Also, reaching similar UV−vis curves as those obtained with Cy−Ge containing solutions requires larger Cy:B ratios as 1:500, yet of lower absorbance. Interestingly, the UV−vis spectrum at lower Cy:B ratios as 1:10 results in two bands: one centered at the same wavelength as the control (535 nm) and the other centered around 592 nm (Figure 2).

This is more evident when UV−vis spectrum of the control solution is subtracted from those of Cy−Md containing solutions, further supporting that with both metalloids there is a notable absorbance increase at 592 nm that would be the responsible of bluer, if so. The resulting spectra (Figures 4 and 5, left) have been also normalized (i.e., for each spectrum, absorbance values are divided by the value of the highest absorbance) to more clearly account for bathochromic shifts (Figures 4 and 5, right).

Two chemical phenomena could explain the absorbance increase at 535 nm when metalloids are added to Cy solutions and both could coexist. On one hand, the Cy−Md complexes formed absorb at nearly the same wavelength as free Cy species in control solutions (*vide infra*). On the other hand, as Cy−Md complexation would remove Cy colored species from equilibria (complexation with colored species is more favorable than that with colorless ones; see below), according to Le Châtelier's principle, the equilibria would be restored by shifting from colorless to colored species increasing absorbance in the visible part of the spectrum.

https://dx.doi.org/10.1021/acs.jafc.0c06827
J. Agric. Food Chem. 2021, 69, 1272−1282

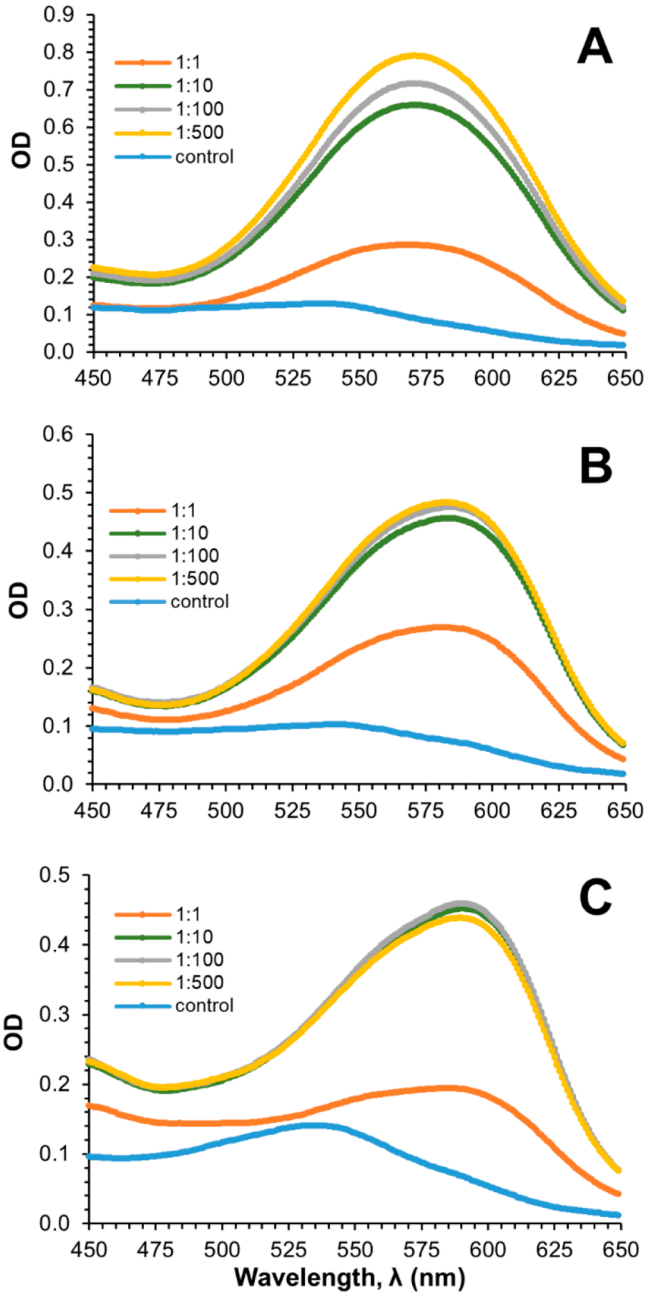

Figure 1. UV−vis spectra for the various cyanidin-based anthocyanins complexed with Ge at different ratios (Cy:Ge). Cy:Ge ratios investigated: 1:1, 1:10, 1:100, and 1:500 at (A) pH 5, (B) pH 6, and (C) pH 7.

Given that more than one species would contribute to the total UV−vis spectra, λ_{max} would be the resulting sum of those contributions. Therefore, absorbance measurements should be performed away from the wavelength of maximum absorbance (at pH 5: Cy−Ge λ_{max} = 571 nm; Cy−B λ_{max} = 566 nm), where the differences in absorbance were the biggest between metalloid containing and control solutions.[45] Thus, we have taken the absorbance value at 592 nm, A_{592}, in all of the experiments. In addition, we have measured the absorbance at 535 nm, A_{535}, (being λ_{max} of control solution at pH 5) for comparison purposes.

An interesting result is found when A_{535}/A_{592} ratios are calculated. In the 1:1 Cy−Ge-containing solution this ratio equals 0.91 while it decreases to 0.81 at the remaining ratios explored. This would explain the shift from purple to blue solutions when jumping from 1:1 to 1:10−1:500 ratios (Figure 2). However, these ratios in Cy−B-containing solutions follow 2, 1.2−1.3 and significantly reduce below 1 at the 1:500 ratio (0.91). Note that at pH 5, the A_{535}/A_{592} ratio equals 2 in the control solution. From these data, it can be inferred that A_{535}/A_{592} ratios below 1 would be required to obtain purple to blue hued solutions.

The increase in absorbance at longer wavelengths as far as 592 nm being responsible for bluer solutions would most likely correspond to formation of any complex of Cy−Ge/B.

Theoretical Results. In order to rationalize at a molecular level the experiments related to visible spectra and provide further information on the molecular structure of the cyanin−metalloid complexes, DFT and TD-DFT calculations were performed.

As reported in the Introduction, color forms of cyanin can be present in solution in cation, neutral, or anion forms whose molar fraction would depend on pH (see below). For neutral and anionic species, different tautomers can be drawn. In a previous work,[46] we have found that the most favored neutral form is that obtained by deprotonation of the hydroxyl group at 4′, **N4′**, (Scheme 1) while two anionic species, obtained by further deprotonation of the hydroxyl group at 7, **A74′**, or at 5, **A54′**, are nearly iso-energetic ($\Delta E_{A54'\rightarrow A74'}$ = 0.43 kcal·mol^{-1}) and would exist in the pH equilibria (Scheme 1). UV−vis spectra have been simulated for all of these uncomplexed Cy forms (Tables 1 and S3). Also, UV−vis spectra of the neutral tautomers resulting from deprotonation at 5, **N5**, and 7, **N7**, have been computed (Table S3).

In addition, we have estimated the proportion of any of the Cy forms at pH 5−7 to determine the mixture of Cy forms in control solutions. This helped us in rationalizing the most likely complex to be formed (see below). Indeed, it is widely accepted that at low pH values (pH > 2) ACNs exist in the cation form as the predominant colored one. However, when pH increases, a mixture of various equilibrium forms would be present. According to previous studies,[47] at pH 5 the mole fraction of the Cy cation, x_C, equals that of the neutral one, x_N, and any significant amount of anions would not be present ($x_C = x_N = 0.5$; $x_A = 0$). Increasing pH would reduce the x_C (0.12 at pH 6 and 0 at pH 7) and increase x_N (0.75 at pH 6 and 0.5 at pH 7) and x_A (0.12 at pH 6 and 0.5 at pH 7). However, in that work, colorless forms were not taken into account as the hydration constant, K_h, was not considered.

When this term is included (pK_h = 3.01)[48] as well as the two estimated acid ionization constants following the strategy reported by León-Carmona et al.[47] (for further details, see the Supporting Information (SI))—that between cation and neutral species, K_{a1}, (pK_{a1} = 4.5) and that between neutral and anion forms, K_{a2}, (pK_{a2} = 7.2) (Scheme 1)—we are able to properly account for more realistic mole fractions.[49] Low mole fractions of the colored species have been obtained (Table 1) indicating that Cy is mainly in its colorless form (Scheme 1), in line with the low absorbance of control solutions in the visible range. Moreover, when summing both simulated UV−vis spectra of the cation and **N4′** supposing $x_C = x_N = 0.5$, the resulting one featured its maximum of absorbance at a wavelength value of 536 nm, being very similar to that of the control solution at pH 5. A similar result (λ_{max} = 540 nm) is obtained when including mole fractions derived from the hydration constant (Table 1), but with this strategy, OD values

https://dx.doi.org/10.1021/acs.jafc.0c06827
J. Agric. Food Chem. 2021, 69, 1272−1282

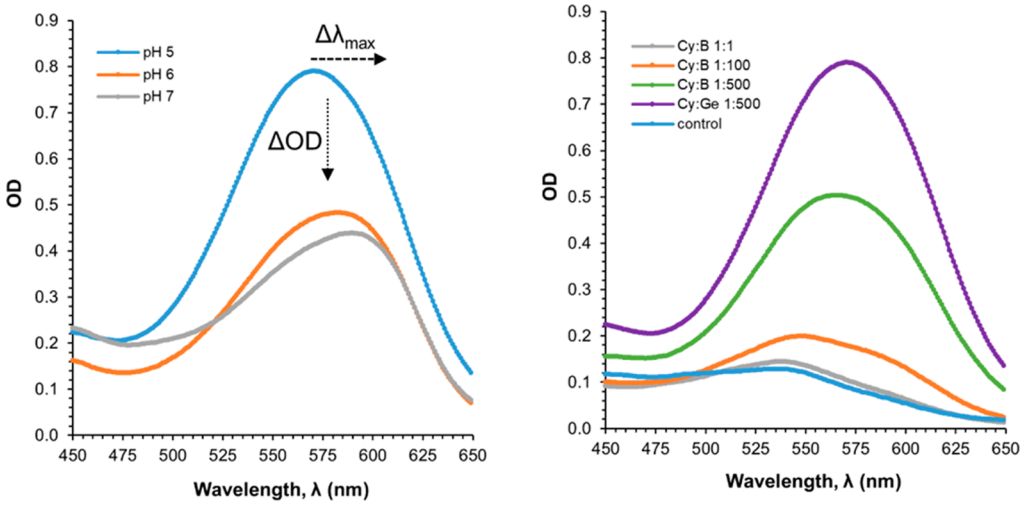

Figure 2. UV−vis spectra for (left) cyanidin-based anthocyanins complexed with Ge at a 1:500 ratio, at the pH values explored (5, 6, and 7) and (right) with B at various Cy:B ratios and comparison with Cy:Ge (1:500) at pH 5.

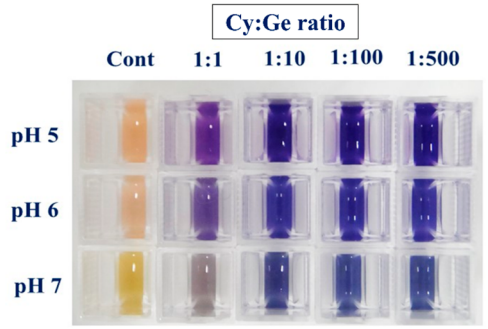

Figure 3. Change in visual appearance of the reaction mixtures of cyanidin-based anthocyanins isolated from Red Rubin sweet basil leaves and Ge ions added with different stoichiometric ratios (1:1, 1:10, 1:100, 1:500; Cy:Ge) at pH 5, 6, and 7.

were more compatible with experimental control solutions obtained here.

Our theoretical results are also in agreement with those reported in an investigation on ACN−Me^{n+} interactions by means of Raman spectroscopy[50] where it was found that Cy at pH 5 is mainly a colorless species, together with small amounts of the red cation and the purple neutral forms.

These previous studies,[24,50,51] further indicate that as metal salts are added to ACN containing solutions, and complexation takes place, the pH dependent equilibria would shift from that of colorless to colored forms increasing absorbance in the visible region. Thus, at first, only colored forms of Cy have been considered for complexation.

According to what is found in the literature, GeO_2 in solution would be present as $Ge(OH)_4$ at the pH values explored experimentally, while boric acid would be as $B(OH)_3$. Possible complexes of cyanin with B and Ge have been explored keeping in mind the following considerations: (i) cyanin acts as a bidentate ligand through the catechol moiety at the B-ring (O3′ and O4′); (ii) only 1:1 complexes have been explored; (iii) only those processes where neutral water is released have been considered.

Bearing all of this in mind, two sets of complexes have been envisioned. Those where $Ge(OH)_4$ (Scheme 2) or $B(OH)_3$ (Scheme 3) lose two (**a1**, **a2**, **a3**) or one (**b1**, **b2**, **b3**) OH group(s). All of them have been optimized, and their corresponding UV−vis spectra have been simulated. The longest absorbance wavelength that otherwise stated matches the maximum absorbance wavelength, λ_{max}, together with the value of the oscillator strength of the transition, f, are depicted in both Schemes 2 and 3. They correspond to the vertical HOMO to LUMO electronic transitions.

Looking at the λ_{max} values depicted in Schemes 2 and 3 and those collected in Table 1, we can observe that, in general, they are similar when comparing any Cy−Md complexes and the Cy form which it derived from (Scheme 4).

Further analysis indeed indicates that at the complex the molecular geometry of the Cy is partially retained. In particular, **b1** resembles the quinoidal-like structure of **N4′** while **a1** is more compatible with that of the Cy cation (Schemes 4 and S2). This is supported by bond lengths: in **b1** C−O4′ (1.30−1.31 Å) is clearly shorter than C−O3′ (1.34−1.35 Å), while in **a1** C−O3′ and C−O4′ distances are longer and similar to each other (1.36−1.37 Å). Together, C2−C1′ distances also go in the same line, being longer in **a1** than in **b1** complexes.[18]

The replacement of O3′-H and O4′-(H) by O3′-B/Ge and O4′-B/Ge induces significant variations of the QTAIM electron charge, $q(\Omega)$, at the O3′ and O4′ atomic basins, q(O3′) and q(O4′), respectively. Indeed, both basins become significantly more negatively charged in **a1**(B) (Δq(O3′) = Δq(O4′) = 0.16 e) while, in **b1**(B), only O3′ experiences such an increase (Δq(O3′) = 0.14 e); q(O4′) remaining substantially unchanged. In contrast, in both **a1**(Ge) and **b1**(Ge), O−Ge bond formation involved charge variations that can be considered comparatively negligible, Δq(O3′/O4′) < 0.04 e. Besides, these oxygen atoms are involved directly in the complexation process, and only the charges at C3′ and, more notably, at C4′ are modified by reducing their positive charges (Δq(C3′) = 0.07 e; Δq(C4′) = 0.17−0.20 e) while the remaining atoms all over the aglycon hold a similar charge.

Concerning oxygen (Cy)−Md distances, O_{Cy}−B distances in **a1** are shorter than those in **b1** (1.39−1.40 Å vs 1.52 (O3′−B)−1.58 (O4′−B) Å). The same is also found in Cy−Ge complexes with O_{Cy}−Ge bond distances (1.80−1.81 Å in **a1** vs 1.85 (O3′−Ge) and 1.97 (O4′−Ge) Å in **b1**). The Cy−Md bonding structure has been also explored by means of QTAIM analysis. Accordingly, electron density properties evaluated at

https://dx.doi.org/10.1021/acs.jafc.0c06827
J. Agric. Food Chem. 2021, 69, 1272−1282

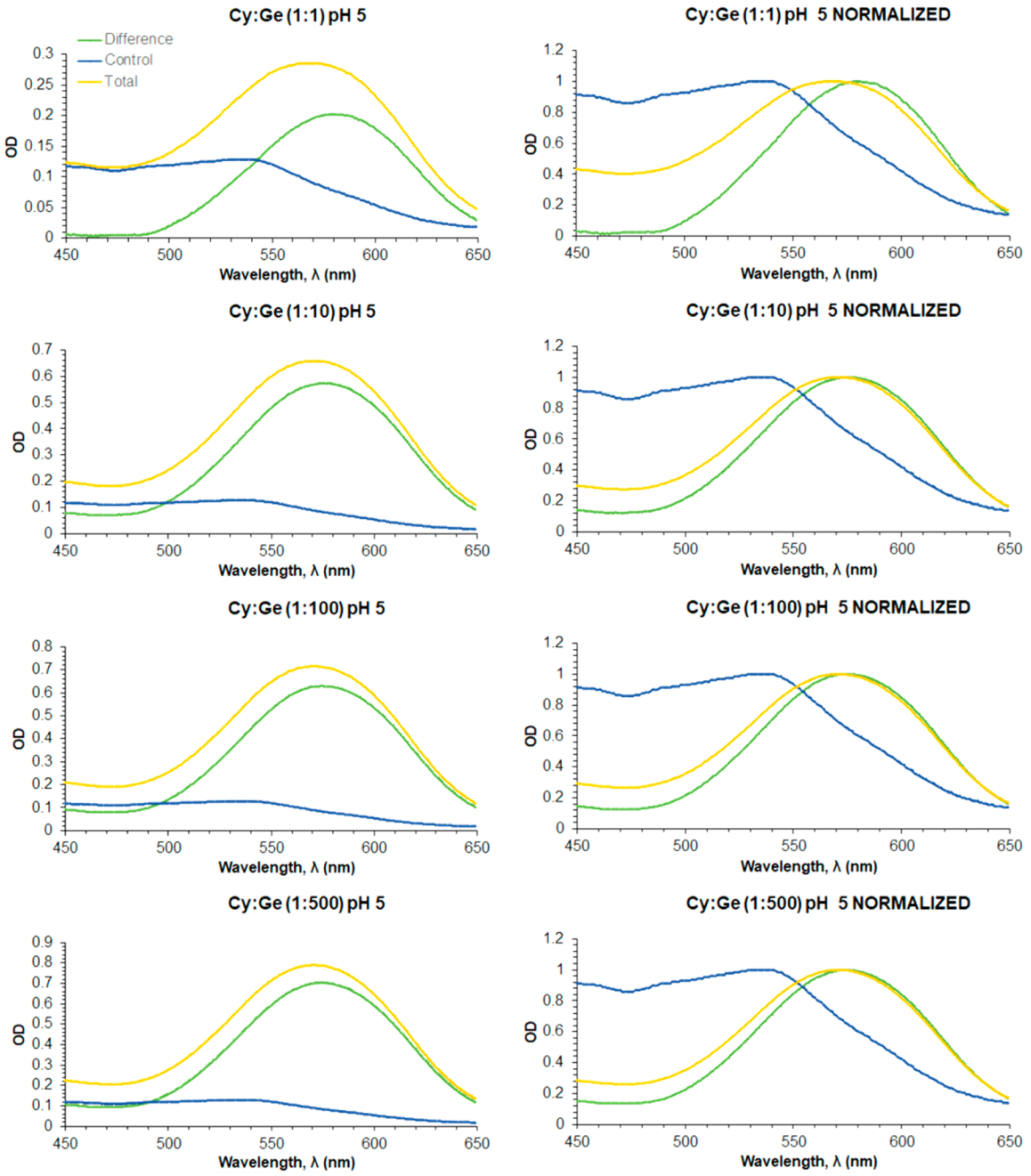

Figure 4. UV−vis spectra of cyanidin-based anthocyanins solutions containing Ge at the various Cy:Ge ratios explored (yellow curves), at pH 5. The curves (green) resulting from subtracting the control solution (blue curves) spectrum (left) are also shown. Normalized curves (right) are also shown to more clearly note bathochromic shifts.

O_{Cy}−Ge/B bond critical points (BCPs), ρ_b—positive $\nabla^2\rho_b$ values and negative but small H_b values of the total energy density (Table S5)—fulfill the hallmarks of bonding to a metal atom. It is further noted that, bearing in mind that δ(A, B) values less than 0.2 indicate the ionic character of the A−B bonding,[52] O_{Cy}−B bonds display a greater ionic character ($\delta(O_{Cy}, B) = 0.4$) than O_{Cy}−Ge ones ($\delta(O_{Cy}, Ge) = 0.6$) in **a1** complexes and that the ionic character increases in **b1** ones, with values of 0.3 and 0.4−0.5, respectively, in **b1**(B) and **b1**(Ge).

Energy of formation for each of the computed Cy−Md complex has been calculated to estimate the most stable one and to compare those of Ge with those of B. Scheme 5 collects the complexation reactions considered here between color forms of Cy with $B(OH)_3$ or $Ge(OH)_4$ leading to the different **a1**−**a3**/**b1**−**b3** complexes (Schemes 2 and 3). ΔE_{solv} values indicate that complexes labeled as **a1**−**a3** are much less favored than **b1**−**b3**. Also, it is clearly shown that complexation with $Ge(OH)_4$ is highly favored over $B(OH)_3$, when comparing the same processes.

For comparison, complexation with hemiacetal and chalcones has been explored. According to our calculations, complexation with colorless forms are not competitive with **b1**−**b3** formation (Table S6) which would reinforce the above related findings, that metal complexation is more favored with colored forms over that with colorless ones. It is of note that

https://dx.doi.org/10.1021/acs.jafc.0c06827
J. Agric. Food Chem. 2021, 69, 1272−1282

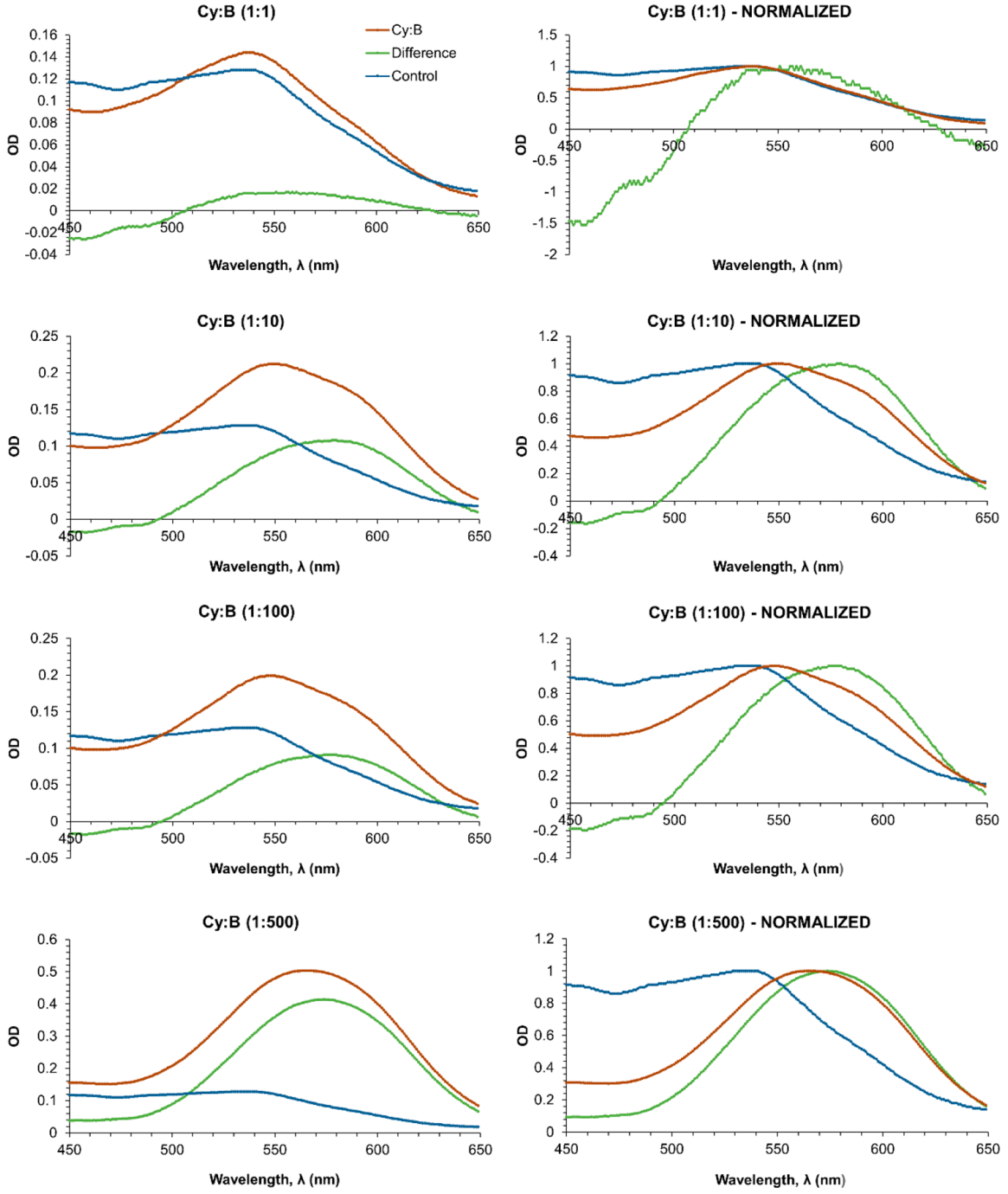

Figure 5. UV−vis spectra of cyanidin-based anthocyanins solutions containing B at the various Cy:B ratios explored (red curves), at pH 5. The curves (green) resulting from subtracting the control solution (blue curves) spectrum (left) are also shown. Normalized curves (right) are also shown to more clearly note bathochromic shifts.

metal complexes with colorless forms remain as colorless complexes.

DISCUSSION

The molecular structure of ACN includes a fully delocalized π-conjugated system. When ACNs bind to metal ions, this decreases the energy needed to cause light-induced electron transition in this chromophore system.[6] Thus, the most distinctive indicators of ACN−Me^{n+} complex formation are the shift of maximum absorption toward longer wavelengths of the visible region (bathochromic shift) and the increase in the intensity of maximal absorbance intensity (so-called hyperchromic effect), which are accompanied by changes of color solution. To date, a great number of the studies have investigated those spectral markers exploring ACN−Me^{n+} complexes,[16,19,31] whereas the possibility that ACN can also bind to Md ions has only been proposed,[16] but it has never been proven experimentally by UV−vis spectroscopy.

Here, larger hyperchromic effects are observed at pH 5 where bathochromic shifts of 35 and 30 nm have been recorded when $Ge(OH)_4$ and $B(OH)_3$ are added, respectively, with λ_{max} values of 571 (Ge) and 566 nm (B). The addition of $Ge(OH)_4$, even at equimolar ratios, to cyanin-containing

https://dx.doi.org/10.1021/acs.jafc.0c06827
J. Agric. Food Chem. 2021, 69, 1272−1282

Table 1. Wavelength of Maximum Absorbance, λ_{max} (nm), Together with the Corresponding Value for the Oscillator Strength, *f*, of the Most Populated Cy Color Species That Could Exist in Acid−Base Equilibria and Mole Fraction Distribution, x_i, of Colored Species at the Different pH Values Tested

	mole fraction,[a] x_i			UV−vis spectra	
Cy species	pH 5	pH 6	pH 7	λ_{max} (nm)	*f*
cation	0.5/*0.0098*	0.12/*0.0010*	0/*0.0001*	524.13	0.8284
neutral **N4′**[b]	0.5/*0.0310*	0.75/*0.0312*	0.5/*0.0307*	544.19	1.2722
neutral **N5**[c]				629.47	0.2975
neutral **N7**				567.15	0.6907
anion **A54′**	0/*0.0002*	0.12/*0.0020*	0.5/*0.0194*	624.08	0.7905
anion **A74′**				621.07	1.1172

[a]In *italics*, mole fraction is expressed in times one, obtained in this work, where hydration constant, K_h, (pK_h = 3.01) has been included (see text). [b]Among the neutral forms, **N4′** is by far the most predominant. [c]λ with maximum absorbance, λ_{max}, does not correspond to the longest one. λ_{max} occurs at 442.2 (*f*: 0.6173).

solutions buffered at pH 5, produces a small pink to violet color change, supporting the idea that complexation is already occurring while a Ge content of 10 × [ACN] resulted in intense blue hues corresponding with the largest bathochromic shift. A larger excess of Ge produces absorbance increases but without further significant shifting of λ_{max}. Thus, the color change induced by the addition of $Ge(OH)_4$ is comparable with that observed with other metals such as Ga^{3+} or Fe^{3+}.[31] In contrast, the addition of $B(OH)_3$ to ACN solutions has little effect on the spectra up to an excess of 500 × [ACN] where the largest bathochromic shift is observed, with similar numbers as those obtained with Cr^{3+},[31] at pH 5 ($\Delta\lambda_{max}$ 30.5 nm with a metal excess of 500 × [ACN]).

When analyzing ACN−Me^{n+} complexation, a sequential complexation mechanism has been proposed, in particular with Al^{3+},[53] where the ACN anion form would be first formed and then complexation with the metal would take place. Another possible mechanism would proceed through concerted steps. Unfortunately, it is not straightforward to dismiss any of them as the ligand molecule, here, Cy, in its anion forms would absorb around the same region as the complexes formed (Table 1 and Schemes 2 and 3). However, neither boric acid nor germanium(IV) acid are expected to be able to remove protons from cation or neutral species to originate anions. Thus, the increasing of absorbance about 592 nm is here assigned to Cy−Md complexes rather than to the Cy anion formation.

Different Cy−Md (Ge/B) complexes have been envisioned, and UV−vis spectra simulations were performed. λ_{max} was very close to that of the uncomplexed Cy from which it comes, suggesting that complexation with these Mds mainly would help in stabilizing the aglycon, which otherwise would suffer from oxidative processes,[8] rather than in substantially modifying its molecular structure (*vide supra*). It has indeed been shown that Cy−Md complexation only leads to marked electron density charge variations at the atoms directly involved in the process: C4′, O3′, O4′, C3′, as noted previously, in Mg^{2+} and Al^{3+} complexes of Cy.[26]

Among the complexes explored, the most feasible ones, obtained when connecting mole fractions (Table 1) and complexation energies (Scheme 4), are those labeled as **b1**, **b2**, and **b3** where Ge is in a pentavalent environment and B is in a tetravalent one. Complexes with Ge have resulted to be largely favored over those with B when the same processes were compared. This would be in line with a large excess of boric acid being required for a significant bathochromic shift, while

Scheme 2. Cyanidin-Based Complexes with Ge (Cy−Ge) Explored with Color Forms of Cyanin[a]

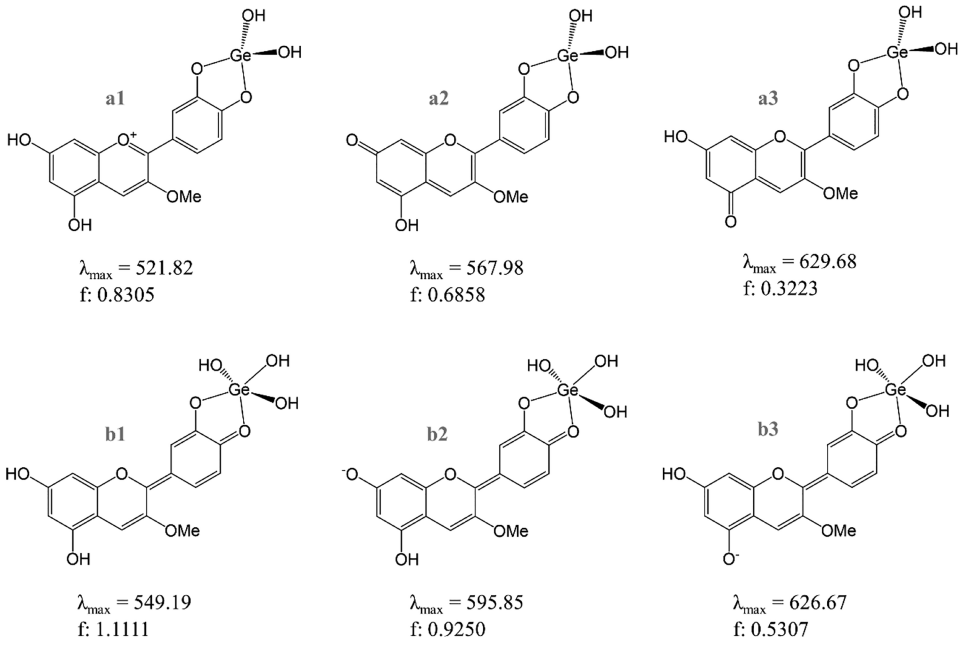

[a]**a1** is obtained from the Cy cation, C; **a2**, **a3**, and **b1** are from **N7**, **N5**, and **N4′**, respectively; and **b2** and **b3** are from **A74′** and **A54′**, respectively. The corresponding wavelength of maximum absorbance, λ_{max}, nm, and oscillator strength, *f*, are shown for each complex.

https://dx.doi.org/10.1021/acs.jafc.0c06827
J. Agric. Food Chem. 2021, 69, 1272−1282

Scheme 3. Cyanidin-Based Complexes with B (Cy−B) Explored with Color Forms of Cyanin[a]

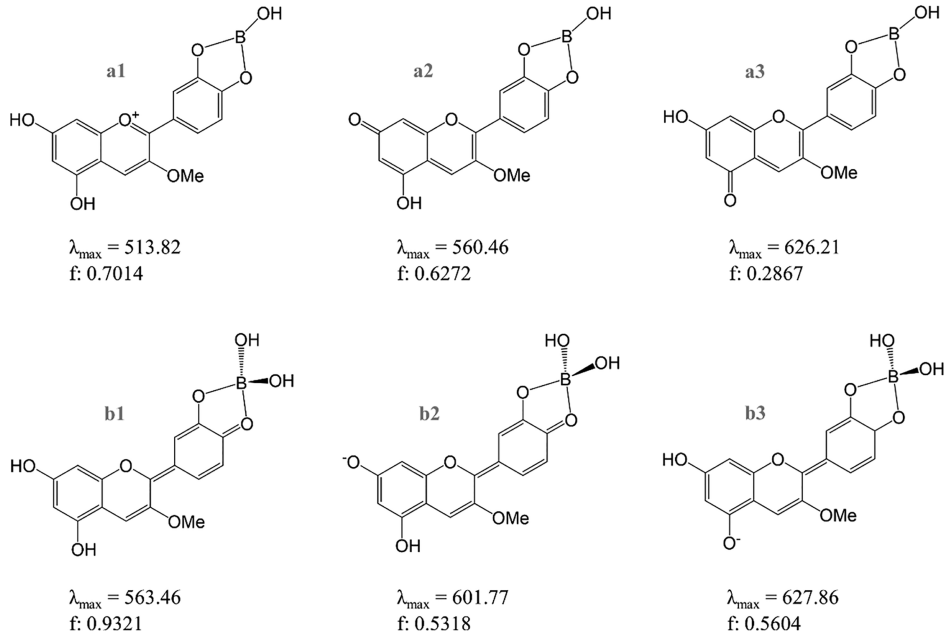

[a]**a1** is obtained from the Cy cation, C; **a2**, **a3**, and **b1** are from **N7**, **N5**, and **N4′**, respectively, and **b2** and **b3** are from **A74′** and **A54′**, respectively. The corresponding wavelength of maximum absorbance, λ_{max}, nm, and oscillator strength, *f*, are shown for each complex.

Scheme 4. Main Resonance Forms of the Aglycon within the Metalloid Complex

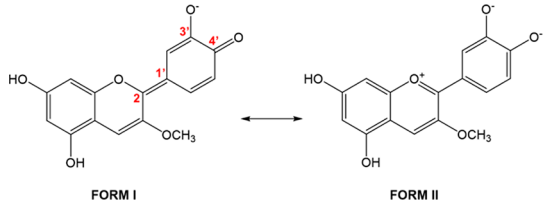

Scheme 5. Main Complexation Reactions Involving Color Forms of Cyanin[a]

➢ **a1** formation from cation, **C**.

$CyH_2^+ + Ge(OH)_4 \rightarrow CyGe(OH)_2^+ + 2H_2O$

ΔE_{solv} = 1.0 kcal·mol^{-1}
ΔG_{solv} = -6.9 kcal·mol^{-1}

$CyH_2^+ + B(OH)_3 \rightarrow CyB(OH)^+ + 2H_2O$

ΔE_{solv} = 11.7 kcal·mol^{-1}
ΔG_{solv} = 0.8 kcal·mol^{-1}

➢ **b1** formation from neutral **N4'**.

$CyH + Ge(OH)_4 \rightarrow CyGe(OH)_3 + H_2O$

ΔE_{solv} = -21.3 kcal·mol^{-1}
ΔG_{solv} = -16.3 kcal·mol^{-1}

$CyH + B(OH)_3 \rightarrow CyB(OH)_2 + H_2O$

ΔE_{solv} = 1.3 kcal·mol^{-1}
ΔG_{solv} = 2.1 kcal·mol^{-1}

➢ **a2/a3** formation from neutral **N5/N7**.

$CyH + Ge(OH)_4 \rightarrow CyGe(OH)_2^+ + 2H_2O$

ΔE_{solv} = 0.8/ 0.9 kcal·mol^{-1};
ΔG_{solv} = -6.9/ -6.8 kcal·mol^{-1}

$CyH + B(OH)_3 \rightarrow CyB(OH)^+ + 2H_2O$

ΔE_{solv} = 10.8 / 10.9 kcal·mol^{-1};
ΔG_{solv} = -0.2/ 0.0 kcal·mol^{-1}

➢ **b2/b3** formation from anions **A54'/ A74'**.

$Cy^- + Ge(OH)_4 \rightarrow CyGe(OH)_3 + H_2O$

ΔE_{solv} = -24.8/ -24.8 kcal·mol^{-1};
ΔG_{solv} = -19.4/ -19.5 kcal·mol^{-1}

$Cy^- + B(OH)_3 \rightarrow CyB(OH)_2 + H_2O$

ΔE_{solv} = -2.0/ -1.7 kcal·mol^{-1};
ΔG_{solv} = -0.7/ -0.3 kcal·mol^{-1}

[a]CyH_2^+ stands for the cation form, CyH stands for any of the three neutral tautomers, and Cy^- stands for any of the anions, giving rise to **a1**−**a3** and **b1**−**b3** complexes. The ΔE_{solv} and ΔG_{solv} (kcal·mol^{-1}) values for corresponding processes are shown.

even with Cy:Ge equimolar ratios a color change occurs and, thus, complexation is already observed. Indeed, Cy−Md formation is shown to be feasible by reaction of the most stable Cy quinoidal base with $Ge(OH)_4$ (ΔE_{solv} = −21.32 kcal·mol^{-1}) though this reaction is slightly unfavorable with $B(OH)_3$ (ΔE_{solv} = 1.28 kcal·mol^{-1}). Moreover, analysis of the electron density of these complexes allowed us to note that O_{Cy}−Ge bonding displays a lower ionic character than O_{Cy}−B bonding, as measured by the computed $\delta(O_{Cy}, M)$ delocalization index. For comparison, a similar ionic bonding character in **b1**−**b3** complexes of B ($\delta(O_{Cy}, B) \sim 0.3$) has been previously noted in $[CyAl(H_2O)_4]^{2+}$ complex ($\delta(O_{Cy}, Al) = 0.2$).[26]

Combining experimental and theoretical results allow us to understand that the visible region of spectra of ACN−Md solutions is the result of more than one absorbent species. A reasonable interpretation of UV−vis spectra of metalloid-containing solutions of Cy is established considering mixtures of mainly **b1**−**b3** complexes, with **b1** as the most likely complex formed (that obtained from **N4′**, the most predominant form at pH 5). In addition, ΔE_{solv} values indicate that **b2** and **b3** complexes (formed by reaction of the metalloid with the anionic quinoidal bases **A54′** and **A74′**) are slightly favored over **b1**. Notably, we have obtained that deprotonation of **b1** leading to **b2** or **b3** is an easier process, with a lower computed pK_a (6.5), than deprotonation of the uncomplexed **N4′** giving rise to **A54′** or **A74′** forms (pK_a (7.2), see the SI). Thus, some amounts of **b2** and **b3** could be present even at pH 5, producing a large red shifting. Together, non-negligible mole fractions of **A54′** and **A74′** anionic species would represent another source of **b2** and **b3** complexes.

When the pH rises from 5 to 7, larger amounts of **b2** and **b3** complexes would be present because of (i) the increasing population of the anion form in control solutions to complex with B/Ge and/or (ii) shifting of the pH equilibria from **b1** to **b2** and **b3**. In this situation, bathochromic shift and hypochromic effects should be noted in the spectra, as **b2** and **b3** feature longer λ_{max} and lower *f* values.

The same explanation would work with B, but with less favored complexation energies. According to $\Delta E_{sol}/\Delta G_{sol}$ values, we can rationalize that complexation with B would require larger excess of $B(OH)_3$ to obtain similar bath-

https://dx.doi.org/10.1021/acs.jafc.0c06827
J. Agric. Food Chem. 2021, 69, 1272−1282

ochromic shifts as with $Ge(OH)_4$. With B, the **b1** complex formation process displays positive ΔE_{solv} and ΔG_{solv} values while those for **b2** and **b3** display slightly negative values. To overcome those unfavorable values, large excesses of the metalloid would force the reaction to proceed.

Overall, based on experimental and theoretical evidence, the elucidation of UV−vis spectra of Cy-containing solutions with metalloid ions, namely Ge and B, is made. Thus, the blue hue is identified mainly with the formation of complexes labeled as **b1**−**b3**, whose mixture at different ratios would produce an increase in absorbance at the wavelength centered around 592 nm. Together, uncomplexed Cy would be contributing to UV−vis spectra of Md-containing Cy solutions, increasing absorbance at a wavelength centered at 535 nm, due to the equilibria shifting from colorless to colored (mainly cation and neutral) forms to globally obtain UV−vis spectra characterized by λ_{max} of 571 (Ge) or 566 (B) nm.

To conclude, the present manuscript highlights for the first time the possibility that two metalloids, namely B and Ge, can complex with anthocyanins, thereby raising the possibility that anthocyanin−metalloid complexation can also occur for other metalloid ions, an aspect which should be considered in future experiments.

■ ASSOCIATED CONTENT

Supporting Information

The Supporting Information is available free of charge at https://pubs.acs.org/doi/10.1021/acs.jafc.0c06827.

> Information of hyperchromic and bathochromic shifts in red basil anthocyanins with pH at different ANC:Md stoichiometry ratios; information on pH equilibria of the uncomplexed cyanidin-3-OMe; strategy followed to estimate the first and second pK_a of Cy; molecular geometry comparison between cation and **N4′** of Cy; selected QTAIM electron density properties of the metalloid−Cy bonding and metalloid complexation with colorless species of Cy (PDF)

■ AUTHOR INFORMATION

Corresponding Authors

Laura Estévez − *Department of Physical Chemistry, University of Vigo, 36310 Vigo, Galicia, Spain;* orcid.org/0000-0001-6191-1500; Email: lestevez@uvigo.es

Marco Landi − *Department of Agriculture, Food and Environment, University of Pisa, I-56124 Pisa, Italy;* orcid.org/0000-0003-0121-0715; Email: marco.landi@unipi.it

Authors

Marta Queizán − *Department of Physical Chemistry, University of Vigo, 36310 Vigo, Galicia, Spain*

Ricardo A. Mosquera − *Department of Physical Chemistry, University of Vigo, 36310 Vigo, Galicia, Spain*

Lucia Guidi − *Department of Agriculture, Food and Environment, University of Pisa, I-56124 Pisa, Italy;* orcid.org/0000-0002-2472-720X

Ermes Lo Piccolo − *Department of Agriculture, Food and Environment, University of Pisa, I-56124 Pisa, Italy*

Complete contact information is available at: https://pubs.acs.org/10.1021/acs.jafc.0c06827

Notes

The authors declare no competing financial interest.

■ ACKNOWLEDGMENTS

L.E. thanks Universidad de Vigo and Xunta de Galicia for financial support and "Centro de Supercomputación de Galicia" (CESGA) for free access to its computational facilities. M.Q. thanks Xunta de Galicia for her predoctoral contract. L.E. and R.A.M. thank Xunta de Galicia for financial support through the project GRC2019/24.

■ REFERENCES

(1) Grotewold, E. The genetics and biochemistry of floral pigments. *Annu. Rev. Plant Biol.* **2006**, *57*, 761−780.

(2) Landi, M.; Tattini, M.; Gould, K. S. Multiple functional roles of anthocyanins in plant-environment interactions. *Environ. Exp. Bot.* **2015**, *119*, 4−17.

(3) Yoshida, K.; Mori, M.; Kondo, T. Blue flower color development by anthocyanins: from chemical structure to cell physiology. *Nat. Prod. Rep.* **2009**, *26*, 884.

(4) Hatier, J. H. B.; Gould, K. S. Anthocyanin function in vegetative organs. In *Anthocyanins: Biosynthesis, Functions, and Applications*; Gould, K. S., Davies, K. M., Winefield, C., Eds.; Springer: New York, 2009; pp 1−20.

(5) Ellestad, G. A. Structure and chiroptical properties of supramolecular flower pigments. *Chirality* **2006**, *18*, 134−144.

(6) Fedenko, V. S.; Shemet, S. A.; Landi, M. UV−vis spectroscopy and colorimetric models for detecting anthocyanin-metal complexes in plants: An overview of in vitro and in vivo techniques. *J. Plant Physiol.* **2017**, *212*, 13−28.

(7) Andersen, Ø. M.; Jordheim, M. The Anthocyanins. In *Flavonoids, Chemistry Biochemistry and Application*; Andersen, O. M., Markham, K. R., Eds.; CRC Press: Boca Raton, FL, 2006; pp 471−552.

(8) Tattini, M.; Landi, M.; Brunetti, C.; Giordano, C.; Remorini, D.; Gould, K. S.; Guidi, L. Epidermal coumaroyl anthocyanins protect sweet basil against excess light stress: multiple consequences of light attenuation. *Physiol. Plant.* **2014**, *152*, 585−598.

(9) Dangles, O.; Fenger, J. A. The chemical reactivity of anthocyanins and its consequences in food science and nutrition. *Molecules* **2018**, *23*, 1970−1992.

(10) Buchweitz, M.; Brauch, J.; Carle, R.; Kammerer, D. R. Application of ferric anthocyanin chelates as natural blue food colorants in polysaccharide and gelatin based gels. *Food Res. Int.* **2013**, *51*, 274−282.

(11) Buchweitz, M.; Brauch, J.; Carle, R.; Kammerer, D. R. Colour and stability assessment of blue ferric anthocyanin chelates in liquid pectin-stabilised model systems. *Food Chem.* **2013**, *138*, 2026−2035.

(12) Sigurdson, G. T.; Giusti, M. M. Bathochromic and hyperchromic effects of aluminum salt complexation by anthocyanins from edible sources for blue color development. *J. Agric. Food Chem.* **2014**, *62*, 6955−6965.

(13) Okoye, C. O. B.; Chukwuneke, A. M.; Ekere, N. R.; Ihedioha, J. N. Simultaneous ultraviolet-visible (UV-vis) spectrophotometric quantitative determination of Pb, Hg, Cd, As and Ni ions in aqueous solutions using cyanidin as a chromogenic reagent. *Int. J. Phys. Sci.* **2013**, *8*, 98−102.

(14) Okoye, C. O. B.; Okon, E. E.; Ekere, N. R.; Ihedioha, J. N. Simultaneous UV-VIS spectrophotometric quantitative determinations of cyanidin complexes of Co, Zn, Cr, Cu, and Fe ions in mixed aqueous solutions. *Int. J. Chem. Anal. Sci.* **2012**, *3*, 1662−1664.

(15) Takeda, K.; Hayashi, K. Metallo anthocyanins. I. Reconstruction of commelinin from its components, awobanin, flavocommelin and magnesium. *Proc. Jpn. Acad., Ser. B* **1977**, *53*, 1−5.

(16) Shiono, M.; Matsugaki, N.; Takeda, K. Structure of the blue cornflower pigment. *Nature* **2005**, *436*, 791.

(17) Landi, M.; Remorini, D.; Pardossi, A.; Guidi, L. Sweet basil (Ocimum basilicum) with green or purple leaves: which differences

occur in photosynthesis under boron toxicity? *J. Plant Nutr. Soil Sci.* **2013**, *176*, 942−951.
(18) Landi, M.; Guidi, L.; Pardossi, A.; Tattini, M.; Gould, K. S. Photoprotection by foliar anthocyanins mitigates effects of boron toxicity in sweet basil (Ocimum basilicum). *Planta* **2014**, *240*, 941−953.
(19) Trouillas, P.; Sancho-García, J. C.; De Freitas, V.; Gierschner, J.; Otyepka, M.; Dangles, O. Stabilizing and modulating color by copigmentation: insights from theory and experiment. *Chem. Rev.* **2016**, *116*, 4937−4982.
(20) Estévez, L.; Sánchez-Lozano, M.; Mosquera, R. A. Complexation of common metal cations by cyanins: Binding affinity and molecular structure. *Int. J. Quantum Chem.* **2019**, *119*, e25834−e25844.
(21) Adamo, C.; Jacquemin, D. The calculations of excited-state properties with Time-Dependent Density Functional Theory. *Chem. Soc. Rev.* **2013**, *42*, 845−856.
(22) Hale, K. L.; Tufan, H. A.; Pickering, I. J.; George, G. N.; Terry, N.; Pilon, M.; Pilon-Smits, E. A. H. Anthocyanins facilitate tungsten accumulation in Brassica. *Physiol. Plant.* **2002**, *116*, 351−358.
(23) Takeda, K.; Kubota, R.; Yagioka, C. Copigments in the blueing of sepal colour of Hydrangea macrophylla. *Phytochemistry* **1985**, *24*, 1207−1209.
(24) Elhabiri, M.; Figueiredo, P.; Toki, K.; Saito, N.; Brouillard, R. Anthocyanin−aluminium and − gallium complexes in aqueous solution. *J. Chem. Soc., Perkin Trans. 2* **1997**, 355−362.
(25) Schreiber, H. D.; Swink, A. M.; Godsey, T. D. The chemical mechanism for Al3+ complexing with delphinidin: A model for the bluing of Hydrangea sepals. *J. Inorg. Biochem.* **2010**, *104*, 732−739.
(26) Estevez, L.; Otero, N.; Mosquera, R. A. Molecular structure of cyanidin metal complexes: Al(III) versus Mg(II). *Theor. Chem. Acc.* **2011**, *128*, 485−495.
(27) Dai, L. P.; Dong, X. J.; Ma, H. H. Antioxidative and chelating properties of anthocyanins in Azolla imbricata induced by cadmium. *Pol. J. Environ. Stud.* **2012**, *21*, 837−844.
(28) Park, W.; Han, K. H.; Ahn, S. J. Differences in root-to-shoot Cd and Zn translocation and by HMA3 and 4 could influence chlorophyll and anthocyanin content in Arabidopsis Ws and Col-0 ecotypes under excess metals. *Soil Sci. Plant Nutr.* **2012**, *58*, 334−348.
(29) Somaatmadja, D.; Powers, J. J.; Hamdy, M. H. Anthocyanins. VI. Chelation studies on anthocyanins and other related compounds. *J. Food Sci.* **1964**, *29*, 655−660.
(30) Buchweitz, M.; Carle, R.; Kammerer, D. R. Bathochromic and stabilising effects of sugar beet pectin and an isolated pectic fraction on anthocyanins exhibiting pyrogallol and catechol moieties. *Food Chem.* **2012**, *135*, 3010−3019.
(31) Sigurdson, G. T.; Robbins, R. J.; Collins, T. M.; Giusti, M. M. Evaluating the role of metal ions in the bathochromic and hyperchromic responses of cyanidin derivatives in acidic and alkaline pH. *Food Chem.* **2016**, *208*, 26−34.
(32) Hale, K. L.; McGrath, S. P.; Lombi, E.; Stack, S. M.; Terry, N.; Pickering, I. J.; George, G. N.; Pilon-Smits, E. A. H. Molybdenum sequestration in Brassica: a role for anthocyanins? *Plant Physiol.* **2001**, *126*, 1391−1402.
(33) *Chemistry of Europe's agricultural soils, part A. Methodology and interpretation of the GEMAS data set*; Reimann, C., Birke, M., Demetriades, A., Filzmoser, P., O'Connor, P., Eds.; Schweizerbart Science Publishers: Germany, 2014.
(34) Wiche, O.; Székely, B.; Moschner, C.; Heilmeier, H. Germanium in the soil-plant system-a review. *Environ. Sci. Pollut. Res.* **2018**, *25*, 31938−31956.
(35) Rosenberg, E. Environmental speciation of germanium. *Ecol. Chem. Eng.* **2007**, *14*, 707−732.
(36) Hayes, J. E.; Pallotta, M.; Baumann, U.; Berger, B.; Langridge, P.; Sutton, T. Germanium as a tool to dissect boron toxicity effects in barley and wheat. *Funct. Plant Bio.* **2013**, *40*, 618−627.
(37) Cakmak, I.; Kurz, H.; Marschner, H. Short-term effects of boron, germanium and high light intensity on membrane permeability in boron deficient leaves of sunflowers. *Physiol. Plant.* **1995**, *95*, 11−18.
(38) Lo Piccolo, E.; Landi, M. Red-leafed species for urban "greening" in the age of global climate change. *J. For. Res.* **2021**, *32*, 151.
(39) Frisch, M. J.; et al. *Gaussian 09*, Revision D.01; Gaussian, Inc., Wallingford CT, 2009.
(40) Tomasi, J.; Mennucci, B.; Cammi, R. Quantum mechanical continuum solvation models. *Chem. Rev.* **2005**, *105*, 2999−3093.
(41) Stratmann, R. E.; Scuseria, G. E.; Frisch, M. J. An efficient implementation of time-dependent density-functional theory for the calculation of excitation energies of large molecules. *J. Chem. Phys.* **1998**, *109*, 8218−8224.
(42) QTAIM Bader, R. F. W. *Atoms in Molecules−A Quantum Theory*; International Series of Monographs in Chemistry, No 22, Oxford University Press: Oxford, 1990.
(43) Bader, R. F. W. A quantum theory of molecular structure and its applications. *Chem. Rev.* **1991**, *91*, 893−928.
(44) Todd, A. K. *AIMAll*, version 16.10.09; TK Gristmill Software, Overland Park KS, USA, 2016.
(45) Dimitrić Marković, J. M.; Veselinović, D. S.; Baranac, J. M.; Brdarić, T. P. Spectroscopic and theoretical study of cyanidin−aluminum (III) complexes. *Spectrosc. Lett.* **2008**, *41*, 104−115.
(46) Estevez, L.; Mosquera, R. A. Conformational and substitution effects on the electron distribution in a series of anthocyanidins. *J. Phys. Chem. A* **2009**, *113*, 9908−9919.
(47) León-Carmona, J. R.; Galano, A.; Alvarez-Idaboy, J. R. Deprotonation routes of anthocyanidins in aqueous solution, pKa values, and speciation under physiological conditions. *RSC Adv.* **2016**, *6*, 53421−53429.
(48) Vidot, K.; Achir, N.; Mertz, C.; Sinela, A.; Rawat, N.; Prades, A.; Dangles, O.; Fulcrand, H.; Dornier, M. Effect of temperature on acidity and hydration equilibrium constants of delphinidin-3-O- and cyaniding-3-O-sambubioside calculated from uni- and multiwavelength spectroscopic data. *J. Agric. Food Chem.* **2016**, *64*, 4139−4145. (b) Dangles, O.; Fenger, J. A. The Chemical reactivity of anthocyanins and its consequences in food science and nutrition. *Molecules* **2018**, *23*, 1970−1992.
(49) Pina, F. Chemical Applications of anthocyanins and related compounds. a source of bioinspiration. *J. Agric. Food Chem.* **2014**, *62*, 6885−6897.
(50) Buchweitz, M.; Gudi, G.; Carle, R.; Kammerer, D. R.; Schulz, H. Systematic investigations of anthocyanin-metal interactions by Raman spectroscopy. *J. Raman Spectrosc.* **2012**, *43*, 2001−2007.
(51) Dangles, O.; Elhabiri, M.; Brouillard, R. Kinetic and thermodynamic investigation of the aluminium−anthocyanin complexation in aqueous solution. *J. Chem. Soc., Perkin Trans. 2* **1994**, 2587−2596.
(52) Schreiber, H. D.; Jones, A. H.; Lariviere, C. M.; Mayhew, K. M.; Cain, J. B. Role of aluminum in red-to-blue color changes in Hydrangea macrophylla sepals. *BioMetals* **2011**, *24*, 1005−1015.

https://dx.doi.org/10.1021/acs.jafc.0c06827
J. Agric. Food Chem. 2021, 69, 1272−1282